communications biology

Article

https://doi.org/10.1038/s42003-024-07021-8

SATB1 prevents immune cell infiltration by regulating chromatin organization and gene expression of a chemokine gene cluster in T cells

Bao Wang [1,2] & Qian Bian [1,2] ✉

SATB1, a key regulator of T cell development, governs lineage-specific transcriptional programs upon T cell activation. The absence of SATB1 has been linked to the initiation and progression of autoimmunity. However, its precise roles in this process remain incompletely understood. Here we show that conditional knockout of *Satb1* in $CD4^+$ T cells in mice led to T cell hyperactivation and inflammatory cell infiltration across multiple organs. Transcriptional profiling on activated T cells revealed that the loss of SATB1 led to aberrant upregulation of CC chemokines. Treating *Satb1* conditional knockout mice with CC chemokine receptor inhibitor alleviated inflammatory cell infiltration. Intriguingly, SATB1's transcriptional regulation of chemokine genes could not be attributed to its direct binding to chemokine promoters. Instead, SATB1 exerted its regulatory effects by controlling higher-order chromatin organization at a CC chemokine locus. The loss of SATB1 led to the emergence of a new chromatin domain encompassing the *Ccl3, Ccl4, Ccl5, Ccl6*, and *Ccl9* genes and a distal enhancer, resulting in increased contacts between the enhancer and all five chemokine genes, thus inducing their upregulation. Collectively, these results demonstrate that SATB1 protects organs from immune cell infiltration by regulating chemokine expression, providing valuable insights into the development of autoimmunity-related phenotypes.

The development, activation, and differentiation of T cells are intricately regulated by numerous transcription factors (TFs) and epigenetic regulators[1]. Key TFs, including BCL11b, NFAT, and GATA3, are activated at different stages of T-cell development and bind to specific DNA motifs, thereby facilitating the transitions between distinct T-cell states[2,3]. These sequence-specific TFs can also recruit epigenetic factors to induce changes in various chromatin modifications such as DNA methylation, histone methylation, and histone acetylation, thereby facilitating the establishment and maintenance of precise gene expression patterns[4]. Interestingly, recent studies have revealed that eukaryotic genomes are organized into a complex hierarchy of 3D architecture including A/B compartments, topologically associating domains (TADs), and promoter–enhancer interactions by the architecture proteins such as cohesin and CTCF, as well as specific TFs[5,6]. Increasing evidence suggests that proper 3D chromatin organization is crucial for gene regulation during T-cell development[7–9], implying that aberrations in chromatin organization may contribute to immune disorders and autoimmunity.

One critical transcriptional regulator that has been linked to both T cell development and autoimmunity is Special AT-rich sequence binding protein 1 (SATB1)[10], which binds to a specific set of AT-rich genomic sequences across the genome[11–14]. SATB1 exerts its regulatory effects on gene expression through multiple mechanisms, including the recruitment of chromatin remodeling complexes such as the NuRD complex to the target regions and the modulation of histone acetylation[15–18]. SATB1 also functions as a global chromatin loop organizer in T cells[19]. Importantly, SATB1 extensively colocalizes with CTCF throughout the genome and influences CTCF-mediated chromatin topology, including many enhancer-promoter interactions, thereby influencing gene expression[20].

It has been reported that in the *Satb1* whole-body knockout mice, T cell development was arrested at the $CD4^+CD8^+$ double-positive stage, and the mice died before sexual maturity[10]. When *Satb1* is conditionally deleted in $CD4^+$ T cells, the mice could survive and reach adulthood[21]. Intriguingly, multiple studies have substantiated the significant role of

[1]Shanghai Institute of Precision Medicine, Ninth People's Hospital, Shanghai Jiao Tong University School of Medicine, Shanghai, China. [2]Shanghai Key Laboratory of Reproductive Medicine, Shanghai Jiao Tong University School of Medicine, Shanghai, China. ✉e-mail: qianbian@shsmu.edu.cn

SATB1 in immune tolerance and the pathogenesis of autoimmune diseases[21–25]. The autoimmunity caused by the *Satb1* deficiency had been attributed to the abnormal development of Treg cells[21]. Indeed, the amount of Treg cells in *Satb1* conditional knockout mice was reduced, particularly at a young age, and reintroduction of normal Treg cells into *Satb1* conditional knockout mice can partially alleviate the autoimmunity-related phenotypes resulting from *Satb1* knockout[22,23]. However, the proportion of Treg cells in the peripheral organs of these mice returned to normal when the mice reached 4 weeks old[21], suggesting other mechanisms besides the development of Treg cells must also contribute to the autoimmunity phenotypes in adult *Satb1* conditional knockout mice. How the loss of SATB1 leads to the occurrence and development of autoimmune diseases, and whether this is related to the misregulation of specific genes, remains to be elucidated.

In this study, we showed that the conditional knockout of *Satb1* in $CD4^+$ T cells (*Satb1* cKO) resulted in T cell hyperactivation and inflammatory cell infiltration, indicative of autoimmunity-related phenotypes. Notably, we found that the expression levels of chemokines *Ccl3, Ccl4, Ccl5, Ccl6*, and *Ccl9*, which are located within a 160 kb genomic neighborhood, exhibit a significant increase in *Satb1* knockout T cells after activation. Administration of chemokine inhibitors reduced the level of inflammatory cell infiltration in *Satb1* knockout mice. Interestingly, the transcriptional regulation of chemokine genes by SATB1 does not involve direct binding to their promoters or modulation of H3K27ac. Rather, we demonstrate that SATB1 orchestrates the appropriate expression of the *Ccl* gene cluster through its control over higher-order chromatin organization and long-range communication between the *Ccl* genes and a prominent transcriptional enhancer (*Ccl*-enhancer). The loss of SATB1 led to the emergence of a new chromatin domain encompassing the *Ccl3*, *Ccl4*, *Ccl5*, *Ccl6*, and *Ccl9* genes and the *Ccl*-enhancer, resulting in increased contacts between the *Ccl*-enhancer and all five chemokine genes, thus inducing their upregulation. Collectively, our data reveal an intricate transcriptional regulatory mechanism by which SATB1 ensures proper *Ccl* gene expression. These findings underscore the critical role of *Satb1* in preserving T cell function, thereby protecting the organisms from immune cell infiltration.

Results

Satb1 knockout led to T cell hyperactivation and inflammatory cell infiltration in mice

To investigate the effect of *Satb1* in T cells, we first crossed $Satb1^{flox/flox}$ mice with *Cd4-Cre* mice to create a $CD4^+$ T cell conditional knockout *Satb1* mouse model (*Satb1* cKO) (Fig. 1a). We found that *Satb1* conditional knockout mice were significantly smaller than their age-matched control littermates (Fig. 1b). Further quantification showed that the *Satb1* conditional knockout mice lost about 20% of their body weight (Fig. 1c). To understand whether such a growth abnormality is linked to aberrations in T cell states and homeostasis in *Satb1* conditional knockout mice, we evaluated the ratio of CD25 and CD69 positive cells on gated $CD4^+$ T cell from control and *Satb1* cKO mice spleen by flow cytometry. We observed that the ratio of CD69 and CD25 positive cells was significantly increased in *Satb1*-knockout T cells (Supplementary Figs. 1 and 2), consistent with previous findings in *Satb1* null mice[10]. Additionally, we also found that compared to the control mice, there was a significant increase in the proportion of $CD44^+$ T cells and a significant decrease in the proportion of $CD62L^+$ T cells in the spleen of *Satb1* cKO mice (Supplementary Fig. 3a–d). Within the $CD44^+$ T cell population, we observed a higher proportion of $CD69^+$ T cells in *Satb1* cKO mice (Supplementary Fig. 3e–g). All these phenomena indicate T cell hyperactivation upon the loss of SATB1. Moreover, consistent with previous reports[21,23], HE staining revealed obvious inflammatory cell infiltration in the lungs and stomachs of *Satb1* cKO mice, but not their control littermates (Supplementary Fig. 4a). Furthermore, the levels of anti-dsDNA autoantibodies in the serum of *Satb1* cKO mice were significantly higher than in the control mice (Supplementary Fig. 4b). Collectively, these data suggest that loss of *Satb1* in $CD4^+$ T cells led to hyperactivation of T cells and infiltration of immune cells into several organs, indicating the emergence of autoimmunity-related phenotypes in mice.

Satb1 knockout caused a significant increase in chemokine gene expression in activated T cells

To further explore the mechanism by which *Satb1* knockout in T cells caused autoimmune disease, naive $CD4^+$ T cells were isolated from the spleen of mice and activated in vitro for 24 h, followed by RNA-Seq to characterize the effect of *Satb1* knockout on the genome-wide expression of activated T cells (Fig. 1d and Supplementary Fig. 5). We found that the knockout of *Satb1* led to a significant change in gene expression of activated T cells, resulting in the up-regulation of 794 genes and the down-regulation of 365 genes (Fig. 1d). Consistent with the hyperactivation phenotype, the up-regulated genes were significantly enriched for genes related to lymphocyte activation and cytokine production pathways (Fig. 1e and Supplementary Fig. 6). Notably, many chemokine family genes, such as *Ccl3*, *Ccl4*, *Ccl5*, *Ccl6*, and *Ccl9*, were significantly upregulated (Fig. 1f). Chemokine factors are mainly composed of CXC, CC, C, and CX3C families, all of which have important implications in autoimmunity. We examined the expression of genes in each family and found that after *Satb1* knockout, there were no significant changes in the expression of genes in the C, CX3C, and CXC families (Fig. 1g). As for the CC gene family, apart from *Ccl3*, *Ccl4*, *Ccl5*, *Ccl6*, and *Ccl9* genes, no other genes showed significant changes (Fig. 1g). Interestingly, these five CC chemokine genes are located within a genomic neighborhood of 160 kb. The elevated expression of these cytokine genes upon the loss of *Satb1* was further confirmed at both transcript and protein levels by performing qPCR (Supplementary Fig. 7a–e) and FACS analysis (Supplementary Fig. 7f, g), respectively.

Notably, while our findings indicate an increase in the expression of *Ccl* chemokine genes in *Satb1*-depleted $CD4^+$ T cells following 24 h activation, Seo et al. observed a decrease in *Ccl5* expression in *Satb1* cKO mouse $CD8^+$ T cells after 5 days of in vitro activation[26]. We confirmed this observation in naive $CD4^+$ T cells using the same experimental setting (Supplementary Fig. 8). However, we noted that the transcriptomes of $CD4^+$ T cells activated for 5 days differ substantially from those of T cells activated for 1 day. To assess the physiological relevance of these different in vitro T cell activation conditions, we examined the expression of *Ccl* genes in tissue-infiltrating T cells in vivo. Immunohistochemical staining revealed a significant amount of CCL3-expressing $CD4^+$ T cells within the lung tissues of *Satb1* cKO mice, whereas those cells are rarely present in wild-type lung tissues (Fig. 1h, i). We further isolated lung-infiltrating $CD4^+$ T cells from control or *Satb1* cKO mice and quantified CC chemokine secretion (Fig. 1j). The infiltrating T cells in *Satb1* cKO mice exhibited higher CCL3 chemokine secretion compared to those in the control group (Fig. 1k). Collectively, these findings and confirmed that *Ccl* gene expression was upregulated in activated T cells upon the loss of *Satb1*, and suggested that the gene expression profiles of the infiltrating T cells in vivo were better recapitulated in the T cells activated for 24 h in vitro than in those activated for a prolonged period.

To further understand the relationship between *Ccl* gene expression and T cell activation, we compared the CC chemokine expression in naive $CD4^+$ T cells from WT and *Satb1* cKO mice before and after activation (Supplementary Fig. 9). Interestingly, among the 5 CC chemokine genes, only *Ccl4* exhibits significant transcriptional upregulation in WT naive $CD4^+$ T cells after activation, while *Ccl5, Ccl6*, and *Ccl9* exhibit transcriptional downregulation after activation, suggesting that these CC chemokine genes are regulated via distinct mechanisms during the normal T cell activation process. However, all 5 CC chemokine genes exhibited increased transcription in activated *Satb1* cKO T cells compared to activated WT T cells, suggesting that SATB1 influences *Ccl* gene expression via a locus-wide mechanism.

Taken together, our results indicate that the knockout of *Satb1* led to the transcriptional upregulation of a specific cluster of CC family chemokine genes in activated $CD4^+$ T cells. The aberrant elevation in chemokines may play an important role in promoting autoimmune diseases and inflammatory cell infiltration in mice.

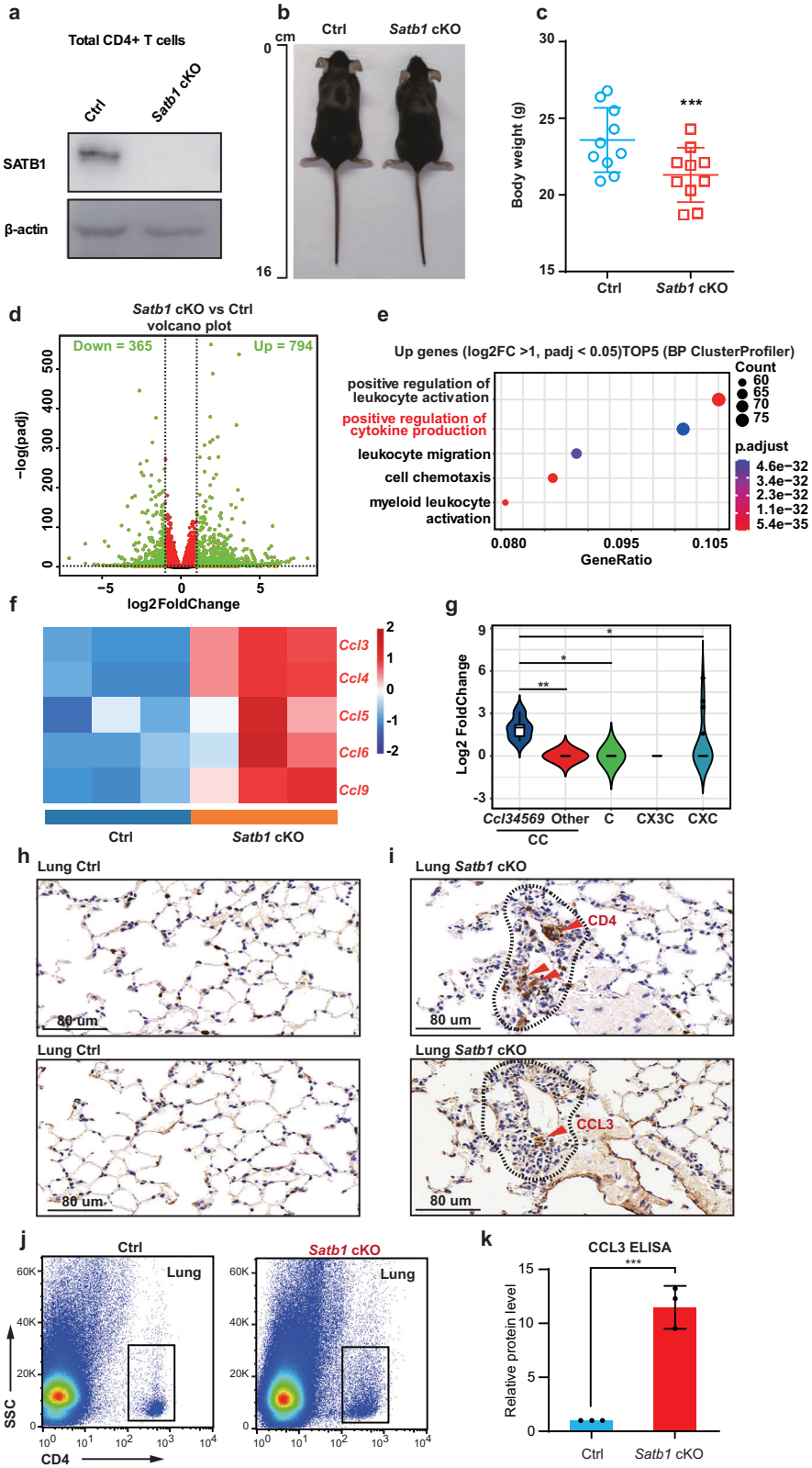

Fig. 1 | Knockout of SATB1 resulted in increased expression of chemokine genes in activated T cells. **a** Western blot shows the efficient depletion of SATB1 in $CD4^+$ T cells. **b** A representative mouse from each group is photographed (6–16 weeks male mice). **c** Statistical comparison of quantified body weight among Ctrl and *Satb1* cKO mice (6–16 weeks male mice, $n = 10$ for each group). Error bars indicate Mean ± SD and each dot represents a mouse. Statistical significance is measured via paired Student's t-tests and is presented as follows: $^{***}p < 0.005$. **d** Volcano plot shows the 365 significantly down-regulated (log2FC < −1 and padj < 0.05) and 794 significantly up-regulated (log2FC > 1 and padj < 0.05) genes in activated naive $CD4^+$ T cells of Ctrl and *Satb1* cKO. About 6–16 weeks male mice were used in this experiment and each group had 3 independent biological replicates. **e** Dot plots indicate the top 5 most enriched BP (biological process) GO terms in up-regulated genes identified in (**a**). **f** Heatmaps of *Ccl3*, *Ccl4*, *Ccl5*, *Ccl6* and *Ccl9* genes. Each column shows the scaled gene expression in an RNA-Seq replicate, each row represents a gene. **g** Violin plots of differentially expressed genes in each chemokine family. Statistical significance is measured via unpaired Student's t-tests and is presented as follows: $^{*}p < 0.05$, $^{**}p < 0.01$, $^{***}p < 0.005$. **h**, **i** Immunohistochemical stainings for CD4 and CCL3 in lung tissues for each group. The representative image shows the lung infiltrating immune cells expressing CD4 and CCL3. **j** Flow cytometric sorting strategy for $CD4^+$ T cells in lung tissues. The lung tissues were digested into single-cell suspension and stained CD4 antibodies for flow cytometric sorting. **k** Protein levels of chemokine CCL3 in lung-infiltrating T cells (sorted from (**g**)) were measured using ELISA ($n = 3$). Statistical significance is measured via unpaired Student's t-tests and is presented as $^{***}p < 0.005$.

Chemokine inhibitor treatment reduced the infiltration of inflammatory cells

Our results showed that the loss of SATB1 led to the aberrant activation of a subset of CC chemokine genes. CC chemokines bind to CC receptors and predominantly recruit mononuclear cells[27,28]. A previous study demonstrated that the aberrant upregulation of CCL2, CCL3, and CCL4 leads to the recruitment of inflammatory cells into the eye and central nervous system, and correlates with the development of autoimmune anterior uveitis (AU) associated with experimental autoimmune encephalomyelitis (EAE)[29]. CC chemokines also contribute to the migration of lymphocytes to the pancreas, impair the function of pancreatic islets, and ultimately lead to the initiation of autoimmune diabetes[30]. To further assess the contribution

of chemokine activation to the autoimmune phenotypes in *Satb1* conditional knockout mice, we examined whether chemokine inhibitor treatment can alleviate inflammatory cell infiltration and organ damage in these mice.

We treated 8-week-old control or *Satb1* conditional knockout mice with the inhibitor of the CCR1 (BX471) and CCR5 (BMS-813160), which are the receptors of CCL3, CCL4, CCL5, and CCL9[31–33]. After being treated with the inhibitors every 3 days for a total of 30 days (Fig. 2a), the lung and stomach tissues of the mice were taken for HE staining. The infiltration of inflammatory cells in the organs of mice was substantially alleviated after the administration of the CCL receptor inhibitor (Fig. 2b, c). Thus, SATB1 protects the organism from infiltration of inflammatory cells partially by repressing the expression of chemokine genes.

SATB1 binds to an enhancer at the *Ccl* locus without affecting its acetylation level

To further understand how the deletion of *Satb1* induced aberrant activation of CC chemokine genes, we performed CUT&Tag to profile the genome-wide occupancy of SATB1 in primary and activated naive $CD4^+$ T cells (Fig. 3a, b). A total of 53,023 and 50,077 SATB1 peaks were identified in primary and activated naive $CD4^+$ T cells, respectively (Supplementary Fig. 10). In both primary and activated naive $CD4^+$ T cells, ~35% of SATB1 peaks colocalize with the promoters of genes. Notably, a significant fraction of SATB1 peaks are located in either introns or intergenic regions, indicating that SATB1 may bind to putative enhancers to regulate transcription (Fig. 3c, d).

We examined the occupancy of SATB1 at the genomic region encompassing *Ccl3, Ccl4, Ccl5, Ccl6*, and *Ccl9*. Although a weak SATB1 peak was found at the promoter of *Ccl4*, SATB1 did not exhibit prominent occupancy at the promoters of other CC chemokine genes (Fig. 3e). Interestingly, a prominent SATB1 peak was observed at an intergenic region ~10 kb downstream of the *Ccl3* gene, raising the possibility that SATB1 may bind to a putative enhancer at the *Ccl* locus (Fig. 3e). Together, our data suggest that SATB1 does not simply regulate *Ccl* gene expression by directly binding to their promoters.

Previous studies have suggested that SATB1 can either upregulate or downregulate histone acetylation levels at its binding sites, thereby influencing gene expression[17]. We conducted H3K27ac CUT&Tag experiments in both control and *Satb1* cKO mouse naive $CD4^+$ T cells to examine the changes in H3K27ac levels, both genome-wide and at the *Ccl* locus (Fig. 4a, b and Supplementary Fig. 11). SATB1 knockout resulted in the upregulation of H3K27 acetylation levels at 4694 sites and downregulation at 3867 sites in naive $CD4^+$ T cells (Fig. 4c). Genes adjacent to the upregulated or downregulated H3K27ac peaks exhibit an overall upregulation or downregulation in their transcription levels, respectively (Fig. 4d), consistent with the known role of H3K27ac in promoting transcription.

At the *Ccl* locus, the H3K27ac levels at the *Ccl3, Ccl4, Ccl5, Ccl6*, and *Ccl9* genes remained largely unaffected following SATB1 knockout, consistent with the lack of SATB1 binding at the promoters of *Ccl* genes (Fig. 4e). Importantly, the SATB1 peaks downstream of the *Ccl3* gene exhibited strong H3K27ac signals, suggesting this site indeed represents an active enhancer, which we designate as *Ccl*-Enhancer (Fig. 4e). However, the H3K27ac level at the *Ccl*-Enhancer was also not affected by the loss of SATB1 binding. Taken together, these multi-omic analyses suggest the transcriptional regulatory effects on the *Ccl* locus exerted by SATB1 are achieved via a mechanism independent of the modulation of H3K27ac levels.

SATB1 regulates *Ccl* gene expression by influencing the enhancer-promoter interactions

In addition to recruiting chromatin-remodeling proteins, recent studies have demonstrated that SATB1 is also an important regulator of the 3D chromatin structure[20,21,34,35]. In particular, our recent study showed that SATB1 can affect the function of chromatin architecture protein CTCF, thereby influencing the organization of chromatin domains and enhancer-promoter interactions[20]. Typically, enhancer-promoter interactions take place within larger chromosomal loop domains anchored by CTCF[36,37]. These loop domains, also known as topologically associating domains (TADs), play a vital role in gene regulation by determining the specificity and frequencies of enhancer-promoter contacts[36,38–40]. Given the intimate link between SATB1 and CTCF, we sought to examine whether the loss of SATB1 disrupts the higher-order chromatin organization at the *Ccl* locus, consequently resulting in changes in *Ccl* expression while minimally affecting the epigenetic modifications.

We compared the chromatin structure at the *Ccl* locus using the previously published Hi-C datasets on wild-type (Ctrl) and *Satb1* knockout thymic T cells[34]. In wild-type T cells, the entire *Ccl* locus is located within a TAD spanning 1.5 Mbp (83.25 Mbp to 84.75 Mbp). Notably, a ~ 250 kb subTAD encompassing the *Ccl* locus appears in *Satb1* knockout T cells (Fig. 5a). Concomitantly, the genomic regions within the new subTAD interact with each other at higher frequencies than with the regions outside the subTAD (Fig. 5b). Notably, this newly emerged subTAD is flanked by two SATB1/ CTCF co-occupied sites that exhibit prominent looping interactions. Upon the depletion of SATB1, the binding of CTCF at these sites (Fig. 5a) and throughout the genome was largely unchanged (Supplementary Fig. 12), consistent with the previous report that SATB1 constrains the interactions between CTCF binding sites without significantly affecting CTCF occupancy[20].

The Hi-C heatmaps at the *Ccl* locus also exhibit a notable increase of signals near the diagonal in *Satb1* cKO thymic T cells, which correspond to shorter-distance chromatin interactions (Fig. 5a). Such an increase in proximal interactions in *Satb1* cKO thymic T cells is also observed in the pile-up heatmap of all TADs (Supplementary Fig. 13), suggesting the ablation of *Satb1* causes chromatin structure changes beyond the *Ccl* locus. For example, we also observed a newly emerged subTAD encompassing the *Ccr* and *Il* loci in *Satb1* cKO thymic T cells (Supplementary Fig. 14), suggesting the misregulation of these genes may also contribute to the autoimmunity-related phenotypes.

Our finding raises a possibility that the formation of the new subTAD encompassing the *Ccl* locus results in elevated interactions between the *Ccl*-Enhancer and the five *Ccl* genes. Notably, *Ccl3* and *Ccl4*, two genes closest to the *Ccl*-Enhancer, exhibit the greatest upregulation in activated *Satb1* cKO T cells (Supplementary Fig. 9). These findings are consistent with our model that the loss of SATB1 remodels the chromatin structure of the *Ccl* locus, causing increased interactions between the *Ccl* genes and the *Ccl*-Enhancer, thereby resulting in elevated transcription for all the *Ccl* genes. To explicitly test this hypothesis, we first quantified the interaction frequencies between the *Ccl*-Enhancer and the promoters of *Ccl3, Ccl4, Ccl5, Ccl6*, and *Ccl9* genes by conducting 3C-qPCR experiments on naive $CD4^+$ T cells obtained from control and *Satb1* conditional knockout mice after 24-hour activation. Indeed, the loss of SATB1 significantly increased the enhancer-promoter interactions at the *Ccl* locus in naive $CD4^+$ T cells (Fig. 5c). To further validate the regulatory function of the *Ccl*-Enhancer, a dCas9-KRAB system was targeted to the *Ccl*-Enhancer in *Satb1* knockout naive $CD4^+$ T cells. By performing qPCR analysis, we show that the silencing of the *Ccl*-Enhancer significantly abrogates the aberrant activation of all five *Ccl* genes (Fig. 5d). Collectively, our data reinforce the notion that SATB1 plays a key role in maintaining the genome organization in T cells. The loss of SATB1 disrupts the large-scale genome organization at the *Ccl* locus and causes aberrant upregulation of *Ccl3, Ccl4, Ccl5, Ccl6*, and *Ccl9* genes, ultimately promoting inflammatory cell infiltration and autoimmunity (Fig. 6).

Discussion

In this study, we have demonstrated the critical role of SATB1, an inner nuclear protein highly expressed in T cells, in protecting against immune cell infiltration by regulating CC chemokine expression. Knocking out *Satb1* in $CD4^+$ T cells leads to increased expression of *Ccl3, Ccl4, Ccl5, Ccl6*, and *Ccl9* genes in T cells, resulting in immune cell infiltration. Mechanistically, these five CC chemokine genes are clustered within a 160 kb genomic neighborhood, with a prominent enhancer (*Ccl*-Enhaner) located 10 kb downstream of the *Ccl3* gene. The knockout of *Satb1* led to the emergence of a new subTAD at this locus, promoting increased interaction frequencies between

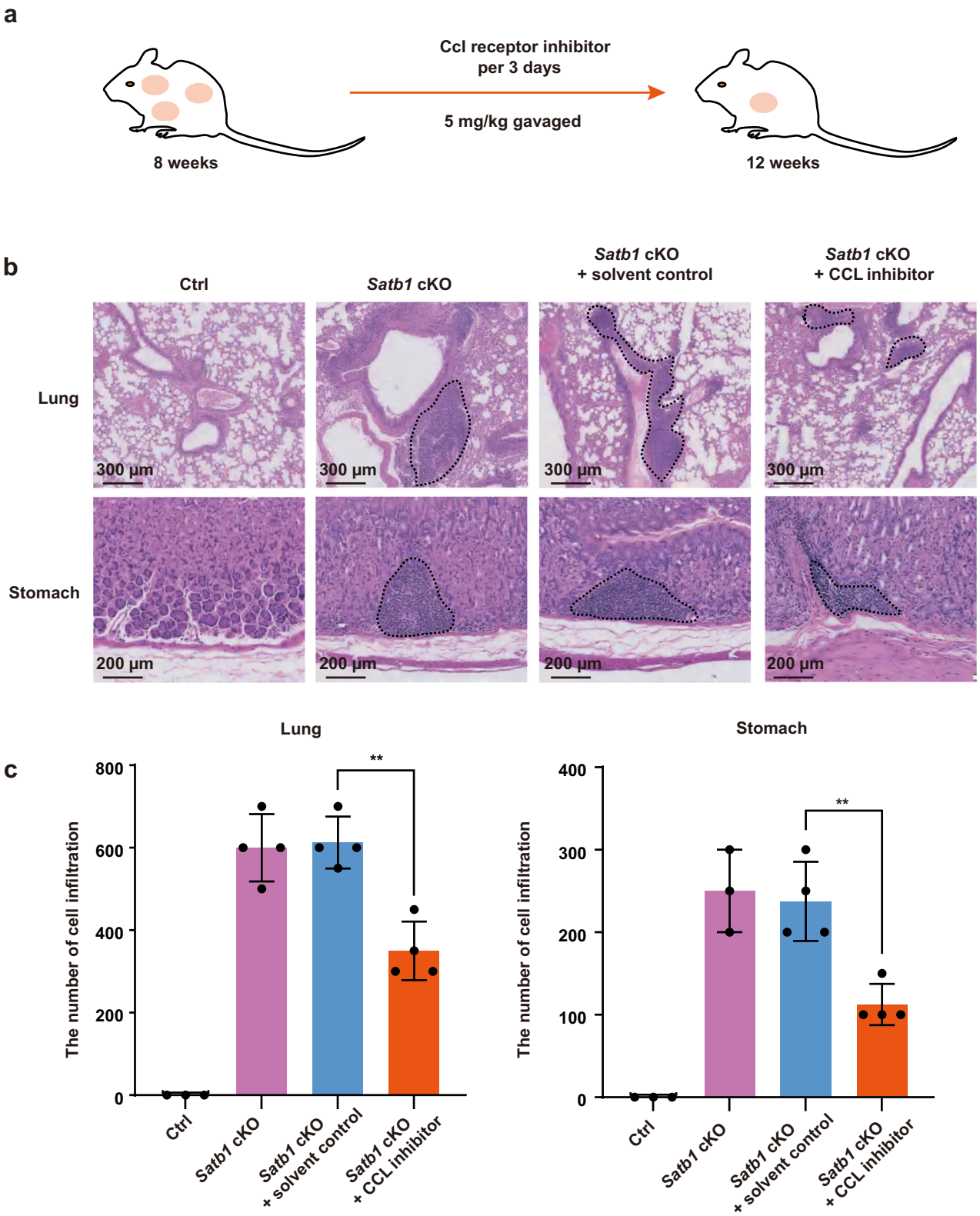

Fig. 2 | Inhibition of CCL chemokines significantly alleviated the infiltration of inflammatory cells in *Satb1* cKO mice. a Schematic presentation of CCR1 and CCR5 inhibition administration into Ctrl and *Satb1* cKO of 8 weeks mice ($n = 6$). **b** HE staining of lung and stomach sections for each group shows that CCR5 inhibition treatment attenuated inflammatory cell infiltration in *Satb1* cKO mice. The immune infiltrated regions were annotated with a black dashed line. **c** Bar chart shows the relative number of inflammatory cells in each group. The number of cells is approximately rounded to the nearest hundred or half-hundred. Error bars indicate Mean ± SD. Statistical significance is measured via unpaired Student's t-tests and is presented as follows: $^{*}p < 0.05$, $^{**}p < 0.01$, $^{***}p < 0.005$.

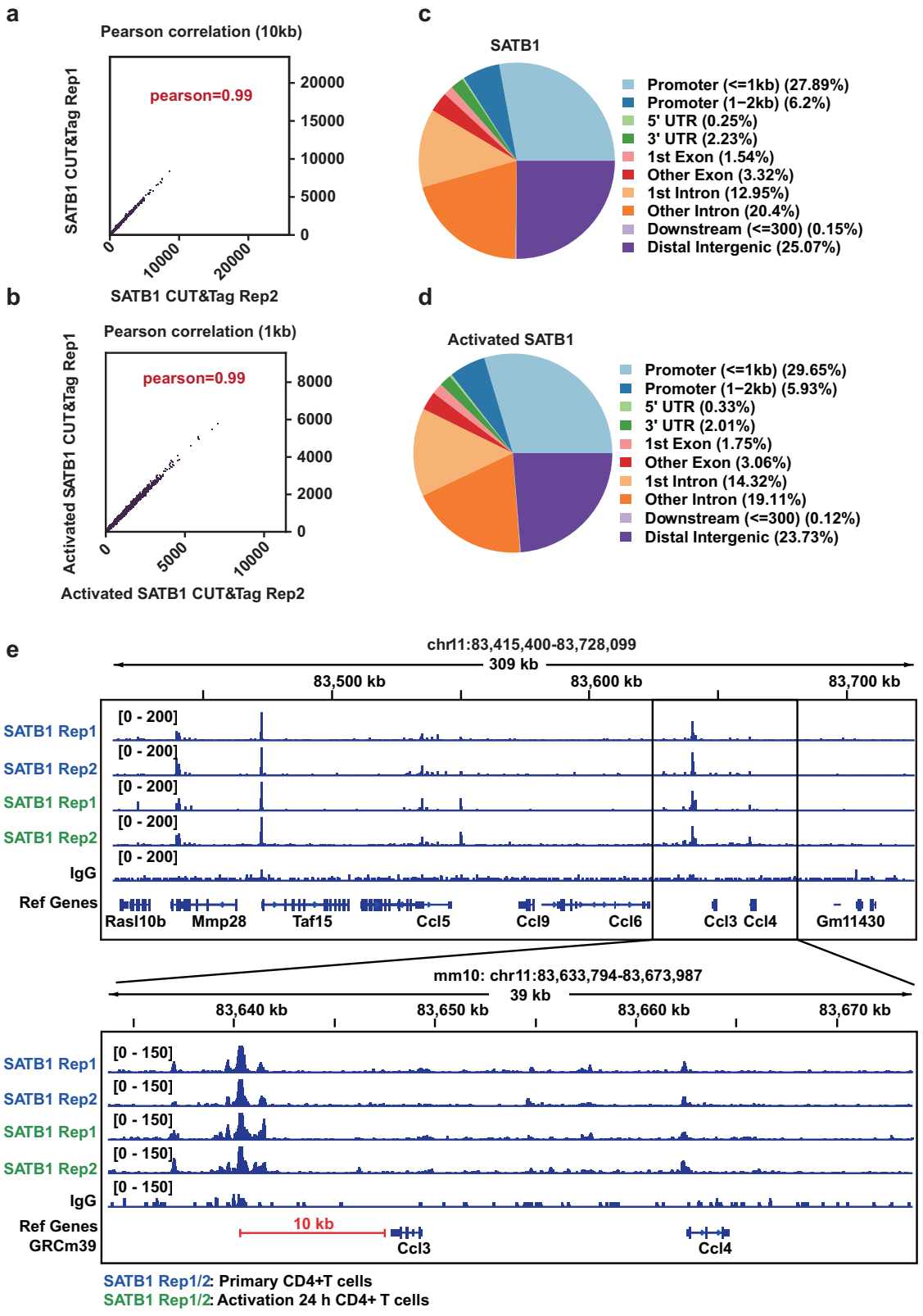

Fig. 3 | The regulatory effects of SATB1 cannot be solely attributed to its binding at the chemokine gene promoter. a Pearson correlation dot plot shows the high reproducibility of CUT&Tag replicates for SATB1 in primary naive $CD4^+$ T cells. **b** Pearson correlation dot plot shows the high reproducibility of CUT&Tag replicates for SATB1 in 24-hour activated naive $CD4^+$ T cells. **c** Pie chart representing the distribution of binding sites in the genome based on the CUT&Tag data from (**a**). **d** Pie chart representing the distribution of binding sites in the genome based on the CUT&Tag data from (**b**). **e** The IGV screenshots revealed the absence of any significant SATB1 binding sites in the *Ccl* gene promoters.

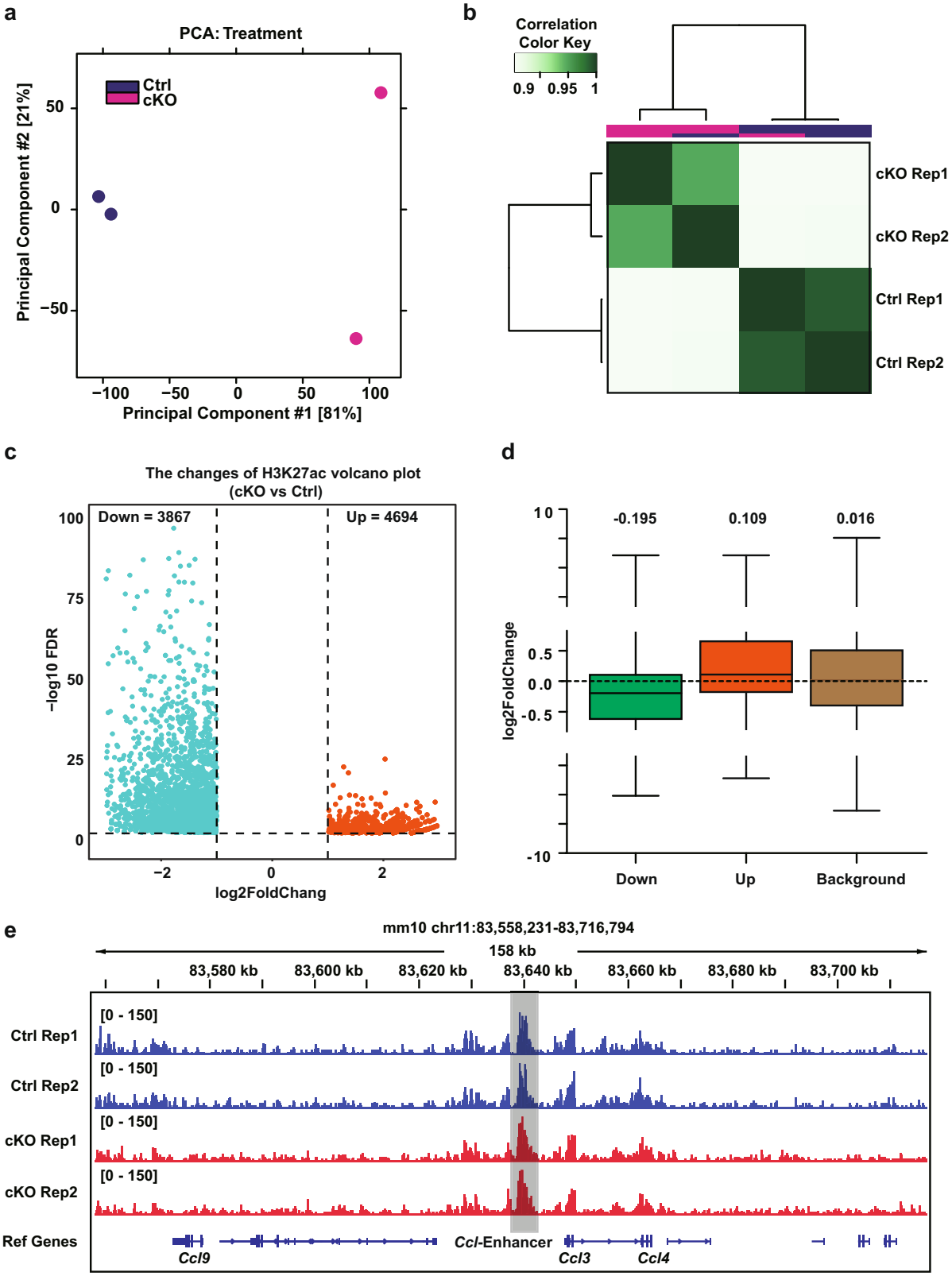

Fig. 4 | SATB1 does not regulate *Ccl* gene expression by influencing H3K27 acetylation levels. a Principle component analysis (PCA) of the samples used for H3K27ac CUT&Tag analysis. **b** Heatmap displaying the correlation of H3K27ac CUT&Tag experiments replicates. **c** Volcano plot showing 8561 differential H3K27ac peaks (4694 up-regulated in red and 3861 down-regulated in blue) between *Satb1* cKO and control mice. **d** Boxplot compares expression changes for genes adjacent to H3K27ac peaks. Genes with peaks of H3K27ac in their promoter regions are classified as genes adjacent to H3K27ac peaks. The median values (-0.195, 0.109, 0.016) are displayed on top of the graphs. **e** H3K27ac signals on the gene cluster sites of *Ccl3, Ccl4, Ccl5, Ccl6*, and *Ccl9* are visualized by IGV software. No significant change was observed in the H3K27ac levels at these sites, while a noticeable enhancer site was identified in the middle of the gene loci of *Ccl3* and *Ccl6*, named as *Ccl*-Enhancer, which was labeled in the gray box.

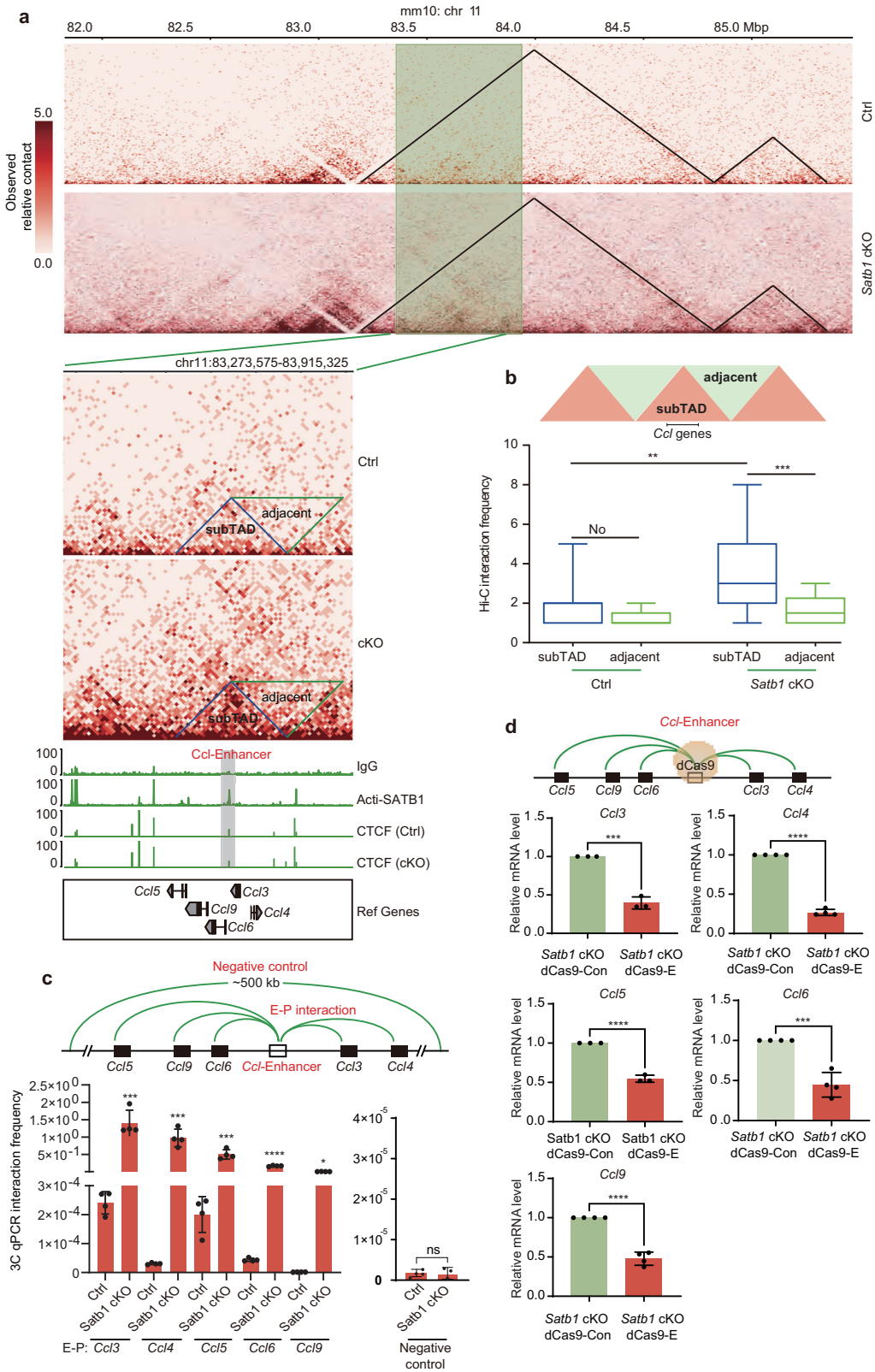

the *Ccl*-Enhancer and the promoters of these CC chemokine genes, thereby causing their aberrant up-regulation. These findings underscore the importance of intricate transcriptional regulatory mechanisms in maintaining the delicate balance of T-cell functions.

Chemokines are crucial in various aspects of host defense, immunosurveillance, and cell recruitment to sites of infection or injury[41,42], and play an important role in the development of autoimmunity[43,44]. There are four major families of chemokines, CXC, CC, C, and CX3C[45], among which the CC chemokines constitute the largest subfamily. Notably, CCL3 and CCL4, two of the most abundant chemokines, are potent chemotactic factors that induce the migration of monocytes and macrophages[46]. The receptor CCR5 plays a pivotal role in responding to CCL3, CCL4, and CCL5 and activating

Fig. 5 | SATB1 regulates the expression of *Ccl* genes by modulating the enhancer-promoter interactions. a Hi-C heatmaps at 10 kb resolution show changed chromatin interactions at *Ccl3, Ccl4, Ccl5, Ccl6*, and *Ccl9* gene loci in thymic T cells. CUT&Tag profiles show the SATB1 and CTCF signals in control and *Satb1* cKO thymocyte cells. The *Ccl*-Enhancer was labeled in the gray box. **b** Diagram depicting the regions of subTAD and adjacent and boxplot showing the interaction frequencies of different regions indicated in (**a**). The adjacent region was set as an internal reference. Error bars indicate Mean ± SD. Statistical significance is measured via unpaired Student's t-tests and is presented as follows: $^{*}p < 0.05$, $^{**}p < 0.01$, $^{***}p < 0.005$. **c** The diagram depicted the 3C-qPCR experiment design and the 3C-qPCR experiment was used to validate the enhancer-promoter interaction of *Ccl3, Ccl4, Ccl5, Ccl6*, and *Ccl9* genes in both control and *Satb1* cKO naive CD4^{+} T cells. A negative control was also detected. Error bars indicate Mean ± SD. Statistical significance is measured via unpaired Student's t-tests and is presented as follows: $^{*}p < 0.05$, $^{**}p < 0.01$, $^{***}p < 0.005$. **d** dCas9 experiment was performed to validate the function of enhancer-promoter interaction in the regulation of gene expression for *Ccl3, Ccl4, Ccl5, Ccl6*, and *Ccl9*. Error bars indicate Mean ± SD. Statistical significance is measured via unpaired Student's t-tests and is presented as follows: $^{*}p < 0.05$, $^{**}p < 0.01$, $^{***}p < 0.005$.

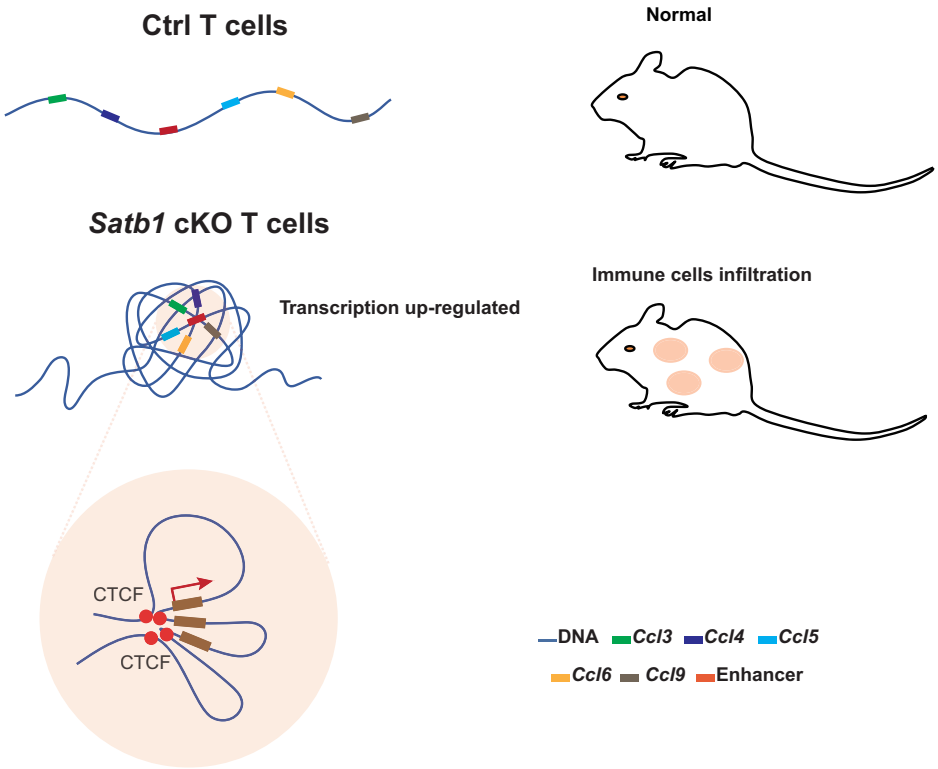

Fig. 6 | Diagram depicting the mechanisms by which SATB1 regulates chemokine gene expression. SATB1 inhibited *Ccl* gene expression by restraining enhancer-promoter interaction. The loss of SATB1 led to the emergence of a new chromatin domain encompassing the *Ccl3, Ccl4, Ccl5, Ccl6*, and *Ccl9* genes and a distal enhancer, which possibly mediated by CTCF, resulting in increased contacts between the enhancer and all five chemokine genes, thus inducing autoimmunity.

Th1 cells during viral infections[47]. CCR5 also plays an important role in inducing immune cells to migrate to the inflamed liver[48]. Furthermore, it has been revealed that CC chemokines contribute to the recruitment of inflammatory cells into the eye, central nervous, and pancreas in various autoimmune diseases[29,30].

In this study, we found that treating *Satb1* cKO mice with a chemokine receptor inhibitor significantly reduces immune cell infiltration into organs, highlighting the potential utility of chemokine receptor inhibitors in clinical therapies for autoimmune diseases. Indeed, some previous studies have demonstrated the therapeutic advantages of targeting CCL chemokines[49,50]. As an example, in Type 1 (insulin-dependent) diabetes mellitus (T1DM), a chronic autoimmune disease, treating Non-Obese Diabetic (NOD) mice with an anti-CCL3 neutralizing antibody has been shown to decrease diabetes incidence[49]. In some cancers, elevated expression of CCL2 facilitates the infiltration of monocytes into tumor tissue, thereby impeding the cytotoxic activity of immune cells against cancer cells[50]. In this context, anti-CCL2 neutralizing antibodies can inhibit the monocyte's infiltration into tumor tissue and constrain tumor growth[50]. However, it is important to note that chemokine function is highly complex, and direct administration of chemokine receptor inhibitors may have intricate outcomes[51]. Thus, further elucidation of the regulatory mechanisms and downstream effects of chemokine will be beneficial for the clinical management of a broad range of autoimmunity-related conditions.

SATB1 plays a crucial role in T cell development[10,21,35]. Multiple previous studies have demonstrated the correlation between *Satb1* and autoimmune diseases[21–23]. The loss of *Satb1* in CD4^{+} T cells causes immune cell infiltration into multiple organs and a significant increase in serum anti-dsDNA autoantibodies[23], which have been partly attributed to the aberrant Treg cell development[21]. Additionally, *Satb1* knockout at the hematopoietic stage in mice recapitulated Sjögren's syndrome[22], an autoimmune disorder that causes dry eyes and mouth. This phenotype could be attributed to elevated levels of indoleamine 2,3-dioxygenase[24]. While the knockout of *Satb1* in T cells from early developmental stages has been linked to autoimmunity, Yasuda et al., reported that the removal of *Satb1* in Th17 cells mitigated the progression of experimental autoimmune encephalomyelitis (EAE)[52], suggesting the pleiotropic effects of *Satb1* in T cell homeostasis and functions. The precise mechanisms by which the deficiency in *Satb1* causes autoimmunity-related phenotypes remain to be elucidated.

Here we show that the aberrant upregulation of the CC chemokine gene cluster serves as a contributing mechanism underlying the inflammatory cell infiltration resulting from the conditional knockout of *Satb1*. By profiling the transcriptome, 3C-qPCR, H3K27ac, and SATB1 occupancy in T cells isolated from the peripheral lymphatic organs of *Satb1* conditional knockout mice, we demonstrated that SATB1 controls the transcription of several critical CC subfamily chemokine genes by maintaining a proper level of promoter-enhancer interaction. The ablation of *Satb1* results in aberrant upregulation of chemokines, promoting inflammatory cell infiltration and

the manifestation of autoimmune phenotypes. These findings highlight SATB1's vital role as a stabilizing factor in preventing the abnormal activation of T cells and protecting organs from immune cell infiltration. It is noteworthy that the etiology of autoimmune diseases resulting from *Satb1* deficiency was previously attributed primarily to aberrant development of Treg cells. However, the involvement of other mechanisms has remained largely unexplored. Our research demonstrates that, in addition to the role of Treg cells, *Satb1* deficiency leads to enhanced chemokine secretion by $CD4^+$ T cells, thereby facilitating immune cell infiltration into target organs and contributing to the pathogenesis and progression of autoimmune diseases. These findings offer novel insights into the molecular mechanisms underlying *Satb1*-induced autoimmune diseases.

Importantly, our results suggest that rather than functioning as a canonical transcriptional factor or epigenetic modification modulator, SATB1 regulates the expression of the *Ccl* cluster by modulating the higher-order chromatin organization. The hierarchical organization of the eukaryotic genome within the nucleus, including A/B compartments, topologically associating domains (TADs), and chromatin loops, is intimately linked to gene expression[6,53–55]. Evidence is accumulating to suggest that chromatin structure plays a significant role in the control of T cell differentiation and activation[56–58]. Our findings further support the notion that dysregulated chromatin structure can lead to abnormal gene expression, impacting T cell development and function, and contributing to immune system imbalances and disease onset. Thus, gaining a deeper understanding of the mechanisms governing higher-order chromatin structure regulation may offer valuable insights and potential therapeutic targets for treating autoimmunity and T-cell-related diseases.

Methods

Satb1 conditional knockout mice and animal models

$Satb1^{flox/flox}$ mice were generated using CRISPR/Cas9 system by Jiangsu Jicui Yaokang Biotechnology Co., Ltd. Briefly, sgRNA-targeting the 3 and 5 introns on both sides of the *Satb1* were constructed and transcribed in vitro. Then, the Cas9 mRNA and the sgRNA will be co-injected into zygotes. Genotyping of all the offspring was performed by PCR. $CD4^+$ T cell-*Satb1* conditional knockout mice were generated by crossing $Satb1^{flox/flox}$ mice with the *Cd4*-Cre mice. The *Cd4*-Cre mice were purchased from Saiye Biotechnology Co., Ltd (Beijing, China). *Cd4*-Cre mice were crossed with $Satb1^{flox/flox}$ mice to generate $Satb1^{flox/flox}$ *Cd4*-Cre mice (*Satb1* conditional knockout (cKO) mice). Control mice consisted of littermates from the same progeny that were either $Satb1^{flox/flox}$ or *Cd4*-Cre mice. Unless specified in the figure legends, mice at the age of 6–16 weeks were used for subsequent experiments. For CCR5 inhibitor treatment, The CCR5 inhibitor (Selleck, S0085) was dissolved in ethanol and administered to mice by oral gavage at a dose of 5 mg/kg every three days for 30 days. All mice used were maintained under specific pathogen-free (SPF) conditions and all experiments were performed following guidelines for animal welfare set by the Animal Welfare Committee of Shanghai Jiaotong University School of Medicine. We have complied with all relevant ethical regulations for animal use.

Naive T cell isolation and activation

Mice were sacrificed by cervical dislocation, and then immediately immersed in 75% alcohol and sterilized for 10 min. Subsequently, the mice were transferred to the biosafety cabinet, the abdominal skin of the mice was cut with ophthalmic scissors, and the mouse spleen was removed with ophthalmic tweezers. The spleen was washed once with PBS, placed in a 40 μm filter (FALCON, Corning, 352340) and ground thoroughly. The cells were lysed with red blood cell lysate for 10 min. After lysate, cells were harvested and resuspended in PBS. Naive T cells were isolated using EasySep™ Mouse naive $CD4^+$ T Cell Isolation Kit (STEMCELL, 19765) according to the manufacturer's instructions. Subsequently, the enriched naive cells underwent antibody staining (CD4-ABflo-594, Abclonal, Cat: A24722; CD25-PE-Cy7, Invitrogen, Cat: 25-0251-82; CD62L-FITC, eBioscience, Cat: 11-0621-81) and the $CD4^+$ $CD25^-$ $CD62L^+$ T cells were sorted as naive $CD4^+$ T cell, as reported previously[59]. For activation, the sorted naive $CD4^+$ T cells were cultured in RPMI-1640 medium, supplemented with 10% FBS, 1% β-mercaptoethanol, and 1% penicillin-streptomycin. Dynabead™ mouse activator CD3/CD28 (Thermofisher, 11453D) was added to the isolated cells, and the cells were activated for 24 h, followed by RNA sequencing, CUT&Tag, RT-qPCR, and 3C-qPCR.

Lung-infiltrating T-cell isolation

Lung tissues from control and *Satb1* cKO mice were isolated and minced with dissection scissors. 1 ml of PBS containing collagenase type II (1.5 mg/ml) was then added to the samples and digested at 37 °C for 1 h. The samples were shaken and mixed every 10 min during this process, with repeated pipetting to accelerate tissue lysis. After digestion, the cells were filtered using a 70 μm cell sieve and collected via centrifugation at 500 g for 5 min. The cells were then resuspended in DPBS and stained with the CD4-ABflo-594 antibody at room temperature for 30 min. The stained cells then underwent fluorescence-activated cell sorting (FACS). About 100,000 $CD4^+$ T cells were collected from both the control and *Satb1* cKO samples. Finally, the sorted cells were lysed and subjected to the ELISA assay to assess the protein level of CCL3.

Hematoxylin and eosin (HE) staining

HE staining was conducted according to the standard protocols. In brief, mice were fixed by transcardiac perfusion with 4% paraformaldehyde and lung and stomach tissues were fixed with 4% paraformaldehyde for 24 h. After fixation, the tissues were then embedded in paraffin. Subsequently, the embedded tissues were dewaxed with xylene for 10 min, followed by anhydrous ethanol for 2 min, 95% ethanol for 1 min, and 75% ethanol for 1 min. The tissues were stained with hematoxylin for 5 min, restained with eosin for 5 min, and mounted with coverslips.

CCR inhibitor treatment

CCR1 inhibitor BX471 (Selleck, S7604) and CCR5 inhibitor BMS-813160 (Selleck, S0085) were purchased from Selleck (Selleck Chemicals, Shanghai, China). BX471 and BMS-813160 were first dissolved in anhydrous ethanol and then diluted 1:20 using phosphate-buffered saline (PBS) to generate 1 μg/μl stock solutions. Mice were then administered a dosage of 5 mg/kg of each inhibitor orally once every three days, continuing for 30 days. Subsequently, the tissues of each group were collected and subjected to hematoxylin and eosin (H&E) staining.

RNA-seq and analysis

RNA-seq libraries were constructed by Anoroad (Beijing, China). Experiments were performed using VAHTS Universal V6 RNA-seq Library Prep Kit for Illumina® (NR604-01/02) according to the manufacturer's instructions. In brief, mRNA was extracted from each sample, and 1–3 μg of each total RNA was purified using poly-T oligo-attached magnetic beads. The mRNA was then fragmented into short nucleotides, and first-strand complementary DNA (cDNA) was synthesized using random hexamer primer, and followed by second-strand cDNA generation. After end repair and 3′-end single nucleotide A (adenosine) addition, the RNA-seq libraries were sequenced on the Illumina Nova Seq 6000 platform at PE150 mode. For RNA-seq data analysis, the sequencing data were aligned to the mouse reference genome (mm10) using the STAR aligner (Dobin et al., 2013) (version 2.7.3a), and all mapped reads were subsequently counted using HTSeq (Anders et al., 2015) (version 0.12.4). The RNA-Seq counts were normalized and stabilized variance using DESeq2 (Love et al., 2014). The differentially expressed genes (DEGs) were identified using a cutoff of abs(log2FC) > 1 and padj < 0.05. Furthermore, GO enrichment analysis was performed using the clusterprofiler (Yu et al., 2012) package (version 4.0.5) in R.

CUT&Tag library preparation

CUT&Tag sample preparation and experiments were performed using the Hyperactive In-Situ ChIP Library Prep Kit for Illumina (Vazyme, TD901-01) as described before (Kaya-Okur et al., 2019) with minimal changes.

Briefly, cells were immobilized using ConA beads. Then, cells were permeabilized and incubated with different primary antibodies (anti-SATB1, Abcam 109122; anti-H3K27ac, Abcam 177178) overnight for 4 °C and then treated with secondary antibodies (Goat anti-Rabbit IgG) for 1 h at room temperature. Afterward, cells were incubated with pG-Tn5 transposase for 1 h and then cells were washed twice and incubated at 37 °C for 1 h. DNA of each sample was extracted using phenol-chloroform-isoamyl alcohol and amplified by PCR. All CUT&Tag libraries were sequenced on the Illumina Nova Seq 6000 platform at PE150 mode.

CUT&Tag data analysis

For CUT&Tag data analysis, raw sequenced fastq data were trimmed using TrimGalore (version 0.6.6) with the default parameters. Trimmed sequence reads were then aligned to the mouse reference genome (mm10) using bowtie2[60] (https://github.com/BenLangmead/bowtie2) with the parameters --very-sensitive -X 2000. Duplicates of mapped reads were removed using sambamba[61] (version 0.8.1). The mapped reads were subsequently shifted before peak calling using the alignmentSieve --ATACshift function from the deepTools package 39 (version 3.3.1). For each CUT&Tag library, we generated the bigwig files at 10 bp bin size using the bamCoverage function from DeepTools and normalized by RPKM. Peak calling for CUT&Tag data was performed using SEACR under the stringent mode with default parameters.

qPCR

RT-qPCR experiments were performed using EZ-press Cell to cDNA Kit PLUS (EZbioscience, B0003) according to the manufacturer's instructions. Briefly, naive $CD4^+$ T cells were activated for 24 h and collected by centrifuge. 400 µl cell lysis buffer was added to the samples. After incubation at room temperature for 5 min, 4 µl of lysates were transferred and 0.8 µl gDNA Remover was added for 5 min. 5 µl 4 × RT Master Mix and 10.2 µl RNase free ddH2O were added to the sample respectively and incubated at 42 °C for 15 min. After the incubation, 4 µl of cDNA was taken out and mixed with 1 µl 10 mM primers and 2 × qPCR buffer. qPCR reactions were performed in a LightCycler 480 II Roche. The Ct values of genes are normalized with the Ct value of β-actin, and then the relative gene expression levels between the treatment group and control group are calculated. The primers used for qPCR are listed in Table 1.

3C-qPCR experiments

3C-qPCR assays were performed as previously described[20,62] with slight modifications. Naive $CD4^+$ T cells isolated from control and *Satb1* cKO mice were activated for 24 h and then cross-linked with 1% formaldehyde. 2.5 M Glycine to the cells to make the final concentration of Glycine 0.2 M. The cells were resuspended with ice-cold Hi-C lysis buffer and incubated for 30 min at room temperature. After lysis, the pellet was resuspended 1x NEB Cutsmart Buffer, and 0.3% final concentration of SDS was added. Samples were incubated for no more than 10 min at 60 °C, followed by another 50 min at 37 °C in a shaker at 750 rpm. Triton X-100 was added to the samples to quench the SDS and digested with EcoRI at 37 °C overnight. The next day, the samples were incubated at 65 °C for 20 min to inactivate the restriction enzyme, and a ligation master mix was added to the samples. After ligation at 16 °C for 4 h in a thermomixer, DNA was purified by standard phenol-chloroform extraction. 3C-qPCR reactions were performed using the Sybr-Greener Kit. A ligation product between two regions ~500 kb apart that do not exhibit interactions above the background was used as the negative control. For all 3C-qPCR experiments, a short-range ligation product formed by two adjacent DpnII restriction fragments was used as an internal standard for normalizing the relative interaction frequencies between genomic regions. The primers used for 3C-qPCR are listed in Table 2.

dCas9 validation

The original dCas9-KRAB plasmid vector was purchased from Addgene (Addgene plasmid #71236) and was replaced with an enhanced green fluorescent protein (eGFP) cassette with PCR (dCas9-KRAB-eGFP plasmid)[62]. sgRNA sequences: 5′- GGTACTGCTCTAATCGTCTAAGG-3′, which target the *Ccl*-Enhancer (Defined in the manuscript) were designed with CHOPCHOP[63] (http://chopchop.cbu.uib.no/). Once the plasmid construction is finished, it is subsequently packaged into a lentivirus. To produce lentivirus, the lentiviral vectors carrying the sgRNA sequences alongside the packaging plasmids psPAX2 and pMD2.G were co-transfected into 293 T cells. The medium was collected daily and filtered. Next, 4× Lenti-X concentrator solution (Clontech, 631231) was added. The medium was incubated at 4 °C overnight and then centrifuged at 3000 × *g* for 20 min at 4 °C. The pellet was collected and then resuspended in 400 µl RPMI-1640. $CD4^+$ T cells were isolated from the spleen and sorted using a Mouse $CD4^+$ T cell separation kit (Selleck, B90001). Specifically, isolated naive T cells are cultured in 12-well plates, with the addition of 20 ng/ml IL-2 and CD3/CD28 magnetic beads activated for 24 h. Subsequently, lentivirus is added to the cells at a ratio of 100 MOI. After 72 hours of infection, cells are sorted for GFP+ cells by flow cytometry, and the sorted cells are collected for qPCR detection.

ELISA experiment for CCL3 detection

CCL3 protein level was determined using Mouse CCL3/MIP-1α ELISA Kit (Liankebio, EK261) according to the manufacturer's instructions. Briefly, the sorted Lung-infiltrating $CD4^+$ T cells isolated from 4 control and 4 *Satb1* cKO mice were lysed with lysis buffer and added to the ELISA reaction plate. CCL3 protein standards at the concentrations of 0, 7.81, 15.63, 31.25, 62.5, 125, 250, and 500 ng/ml were also added to the reaction plate to create a standard curve. Absorbance for each well was detected using a microplate reader, and the concentration of CCL3 in each sample was calculated. The fold change in CCL3 concentration was determined by dividing the concentration in the *Satb1* cKO mice samples by the concentration in the control mice samples.

Anti-dsDNA autoantibody detection

Concentrations of anti-dsDNA autoantibodies in the serum were measured using a Mouse anti-dsDNA antibody ELISA Kit (CUSABIO, CSB-E11194m) according to the manufacturer's instructions. Briefly, blood was drawn from the eyeballs of 4 control and 3 *Satb1* cKO mice, left at room temperature for 1 h, and then centrifuged at 1000 × *g* for 10 min. The precipitate was discarded and the supernatant was collected as serum. The serum was then added to an ELISA reaction plate. Anti-dsDNA antibody (IgG) standards at the concentrations of 2.5, 5, 10, and 20 ng/ml were used to create a standard curve for determining the autoantibody concentrations in the serum.

Table 1 | Primers for RT-qPCR

Gene name	Forward primer (5′-3′)	Reversed primer (5′-3′)
CCL3	ACTGCCTGCTGCTTCTCCTACA	ATGACACCTGGCTGGGAGCAAA
CCL4	ACCCTCCCACTTCCTGCTGTTT	CTGTCTGCCTCTTTTGGTCAGG
CCL5	CCTGCTGCTTTGCCTACCTCTC	ACACACTTGGCGGTTCCTTCGA
CCL6	CACCAGTGGTGGGTGCATCAAG	GTGCTTAGGCACCTCTGAACTC
CCL9	TCCAGAGCAGTCTGAAGGCACA	CCGTGAGTTATAGGACAGGCAG
β-actin	CATTGCTGACAGGATGCAGAAGG	TGCTGGAAGGTGGACAGTGAGG

Table 2 | Primers for 3C-qPCR

E-P name	Forward primer (5′-3′)	Reversed primer (5′-3′)
CCL3	GAAGGGAAGGTCTTTGCCACTAC	CTCACAGGCCCATCTCACAAG
CCL4	GAAGGGAAGGTCTTTGCCACTAC	GGAGGAATTAAGGGTAGATAGG
CCL5	TAACCTGGTGCCACTCACAAAG	CACTGGTGACAGATATGAGC
CCL6	TAACCTGGTGCCACTCACAAAG	CTGCTATTGACGTCTTTTCTG
CCL9	TAACCTGGTGCCACTCACAAAG	GCTGCTTTTTGTCAGTATATAGG
Normalize control	ACACAATGGAGCGCTACTCAG	GTATCTTGGGTATTCTAAG
Negative control	AGCCACAAGAGAGTTAGTAGTAC	GCTCTCTAAACCCAGTTTTGCCATC

Statistics and reproducibility

All bar plots are presented as Mean ± SD, with individual data points shown. Statistics were calculated on samples containing three or more replicates from independent experiments. *P*-values were calculated using either the unpaired t-test or the Wald test, as indicated in figure legends.

Data availability

All data supporting the findings within this study are available in Supplementary Information. All source data for graphs in this study are provided in the Supplementary Data file. Uncropped blot images are provided in Supplementary Information (Supplementary Fig. 15). High-throughput sequencing data and processed files used in this study have been deposited in the National Center for Biotechnology Information (NCBI) Gene Expression Omnibus (GEO) under accession number GSE224977. Other analysis codes and additional raw data required to reanalyze the data reported in this paper are available from the lead contact upon reasonable request.

Received: 14 March 2024; Accepted: 5 October 2024;
Published online: 11 October 2024

References

1. Chiara, V. D., Daxinger, L. & Staal, F. The route of early T cell development: crosstalk between epigenetic and transcription factors. *Cells*. **10**, 1074 (2021).
2. Kuo, C. T. & Leiden, J. M. Transcriptional regulation of T lymphocyte development and function. *Annu. Rev. Immunol.* **17**, 149–187 (1999).
3. Zhong, Y. et al. Hierarchical regulation of the resting and activated T cell epigenome by major transcription factor families. *Nat. Immunol.* **23**, 122–134 (2022).
4. Pace, L. & Amigorena, S. Epigenetics of T cell fate decision. *Curr. Opin. Immunol.* **63**, 43–50 (2020).
5. Rowley, M. J. & Corces, V. G. Organizational principles of 3D genome architecture. *Nat. Rev. Genet.* **19**, 789–800 (2018).
6. Zheng, H. & Xie, W. The role of 3D genome organization in development and cell differentiation. *Nat. Rev. Mol. Cell Biol.* **20**, 535–550 (2019).
7. Pongubala, J. & Murre, C. Spatial organization of chromatin: transcriptional control of adaptive immune cell development. *Front. Immunol.* **12**, 633825 (2021).
8. Papadogkonas, G., Papamatheakis, D. A. & Spilianakis, C. 3D genome organization as an epigenetic determinant of transcription regulation in T cells. *Front. Immunol.* **13**, 921375 (2022).
9. Zhao, X., Zhu, S., Peng, W. & Xue, H. H. The interplay of transcription and genome topology programs T cell development and differentiation. *J. Immunol.* **209**, 2269–2278 (2022).
10. Alvarez, J. D. et al. The MAR-binding protein SATB1 orchestrates temporal and spatial expression of multiple genes during T-cell development. *Genes Dev.* **14**, 521–535 (2000).
11. Kuwabara, T. et al. SATB1-dependent mitochondrial ROS production controls TCR signaling in CD4 T cells. *Life Sci. Alliance*. **4**, e202101093 (2021).
12. Patta, I. et al. Dynamic regulation of chromatin organizer SATB1 via TCR-induced alternative promoter switch during T-cell development. *Nucleic Acids Res.* **48**, 5873–5890 (2020).
13. Nakayama, Y., Mian, I. S., Kohwi-Shigematsu, T. & Ogawa, T. A nuclear targeting determinant for SATB1, a genome organizer in the T cell lineage. *Cell Cycle* **4**, 1099–1106 (2005).
14. Kakugawa, K. et al. Essential roles of SATB1 in specifying T lymphocyte subsets. *Cell Rep.* **19**, 1176–1188 (2017).
15. Kumar, P. P., Purbey, P. K., Ravi, D. S., Mitra, D. & Galande, S. Displacement of SATB1-bound histone deacetylase 1 corepressor by the human immunodeficiency virus type 1 transactivator induces expression of interleukin-2 and its receptor in T cells. *Mol. Cell. Biol.* **25**, 1620–1633 (2005).
16. Stephen, T. L. et al. SATB1 expression governs epigenetic repression of PD-1 in tumor-reactive T cells. *Immunity* **46**, 51–64 (2017).
17. Yasui, D., Miyano, M., Cai, S., Varga-Weisz, P. & Kohwi-Shigematsu, T. SATB1 targets chromatin remodelling to regulate genes over long distances. *Nature* **419**, 641–645 (2002).
18. Pavan, K. P. et al. Phosphorylation of SATB1, a global gene regulator, acts as a molecular switch regulating its transcriptional activity in vivo. *Mol. Cell.* **22**, 231–243 (2006).
19. Cai, S., Lee, C. C. & Kohwi-Shigematsu, T. SATB1 packages densely looped, transcriptionally active chromatin for coordinated expression of cytokine genes. *Nat. Genet.* **38**, 1278–1288 (2006).
20. Wang, B., Ji, L. & Bian, Q. SATB1 regulates 3D genome architecture in T cells by constraining chromatin interactions surrounding CTCF-binding sites. *Cell Rep.* **42**, 112323 (2023).
21. Kitagawa, Y. et al. Guidance of regulatory T cell development by Satb1-dependent super-enhancer establishment. *Nat. Immunol.* **18**, 173–183 (2017).
22. Tanaka, Y. et al. SATB1 conditional knockout results in Sjogren's syndrome in mice. *J. Immunol.* **199**, 4016–4022 (2017).
23. Kondo, M. et al. SATB1 plays a critical role in establishment of immune tolerance. *J. Immunol.* **196**, 563–572 (2016).
24. Tanaka, Y. et al. Increased indoleamine 2,3-dioxygenase levels at the onset of Sjogren's syndrome in SATB1-conditional knockout mice. *Int. J. Mol. Sci*. **22**, 10125 (2021).
25. Akiba, Y., Kuwabara, T., Mukozu, T., Mikami, T. & Kondo, M. Special AT-rich sequence binding protein 1 is required for maintenance of T cell receptor responsiveness and development of experimental autoimmune encephalomyelitis. *Microbiol. Immunol.* **62**, 255–268 (2018).
26. Seo, W. et al. Runx-mediated regulation of CCL5 via antagonizing two enhancers influences immune cell function and anti-tumor immunity. *Nat. Commun.* **11**, 1562 (2020).
27. Fabisiak, J. P. et al. Mycoplasma fermentans and TNF-beta interact to amplify immune-modulating cytokines in human lung fibroblasts. *Am. J. Physiol. -Lung Cell. Mol. Physiol.* **291**, L781–L793 (2006).
28. Strieter, R. M., Belperio, J. A. & Keane, M. P. Cytokines in innate host defense in the lung. *J. Clin. Invest.* **109**, 699–705 (2002).
29. Adamus, G., Manczak, M. & Machnicki, M. Expression of CC chemokines and their receptors in the eye in autoimmune anterior

uveitis associated with EAE. *Investig. Ophthalmol. Vis. Sci.* **42**, 2894–2903 (2001).
30. Lin, G. J. et al. Transgenic expression of murine chemokine decoy receptor D6 by islets reveals the role of inflammatory CC chemokines in the development of autoimmune diabetes in NOD mice. *Diabetologia* **54**, 1777–1787 (2011).
31. Norman, P. A dual CCR2/CCR5 chemokine antagonist, BMS-813160? Evaluation of WO2011046916. *Expert Opin. Ther. Pat.* **21**, 1919–1924 (2011).
32. Liang, M. et al. Identification and characterization of a potent, selective, and orally active antagonist of the CC chemokine receptor-1. *J. Biol. Chem.* **275**, 19000–19008 (2000).
33. Feng, S. et al. Therapeutic effect of C-C chemokine receptor type 1 (CCR1) antagonist BX471 on allergic rhinitis. *J. Inflamm. Res.* **13**, 343–356 (2020).
34. Zelenka, T. et al. The 3D enhancer network of the developing T cell genome is shaped by SATB1. *Nat. Commun.* **13**, 6954 (2022).
35. Feng, D. et al. Chromatin organizer SATB1 controls the cell identity of CD4(+) CD8(+) double-positive thymocytes by regulating the activity of super-enhancers. *Nat. Commun.* **13**, 5554 (2022).
36. Tang, Z. et al. CTCF-mediated human 3D genome architecture reveals chromatin topology for transcription. *Cell* **163**, 1611–1627 (2015).
37. Davidson, I. F. et al. CTCF is a DNA-tension-dependent barrier to cohesin-mediated loop extrusion. *Nature* **616**, 822–827 (2023).
38. Hnisz, D., Day, D. S. & Young, R. A. Insulated neighborhoods: structural and functional units of mammalian gene control. *Cell* **167**, 1188–1200 (2016).
39. Dixon, J. R. et al. Topological domains in mammalian genomes identified by analysis of chromatin interactions. *Nature* **485**, 376–380 (2012).
40. Lupianez, D. G. et al. Disruptions of topological chromatin domains cause pathogenic rewiring of gene-enhancer interactions. *Cell* **161**, 1012–1025 (2015).
41. Olson, T. S. & Ley, K. Chemokines and chemokine receptors in leukocyte trafficking. *Am. J. Physiol. Regul. Integr. Comp. Physiol.* **283**, R7–R28 (2002).
42. Moser, B. & Loetscher, P. Lymphocyte traffic control by chemokines. *Nat. Immunol.* **2**, 123–128 (2001).
43. Meitei, H. T., Jadhav, N. & Lal, G. CCR6-CCL20 axis as a therapeutic target for autoimmune diseases. *Autoimmun. Rev.* **20**, 102846 (2021).
44. Antonelli, A. et al. Chemokine (C-X-C motif) ligand (CXCL)10 in autoimmune diseases. *Autoimmun. Rev.* **13**, 272–280 (2014).
45. Zlotnik, A. & Yoshie, O. Chemokines: a new classification system and their role in immunity. *Immunity* **12**, 121–127 (2000).
46. Ahmadabadi, B. N. et al. Downregulation of CCR5 expression on the peripheral blood CD8+ T cells of southeastern Iranian patients with chronic hepatitis B infection. *Inflammation* **36**, 136–140 (2013).
47. Crane, I. J. et al. Involvement of CCR5 in the passage of Th1-type cells across the blood-retina barrier in experimental autoimmune uveitis. *J. Leukoc. Biol.* **79**, 435–443 (2006).
48. Ajuebor, M. N., Carey, J. A. & Swain, M. G. CCR5 in T cell-mediated liver diseases: what's going on? *J. Immunol.* **177**, 2039–2045 (2006).
49. Cameron, M. J. et al. Differential expression of CC chemokines and the CCR5 receptor in the pancreas is associated with progression to type I diabetes. *J. Immunol.* **165**, 1102–1110 (2000).
50. Izhak, L. et al. Predominant expression of CCL2 at the tumor site of prostate cancer patients directs a selective loss of immunological tolerance to CCL2 that could be amplified in a beneficial manner. *J. Immunol.* **184**, 1092–1101 (2010).
51. Cecchinato, V., Martini, V., Pirani, E., Ghovehoud, E. & Uguccioni, M. The chemokine landscape: one system multiple shades. *Front. Immunol.* **14**, 1176619 (2023).
52. Yasuda, K. et al. Satb1 regulates the effector program of encephalitogenic tissue Th17 cells in chronic inflammation. *Nat. Commun.* **10**, 549 (2019).
53. Dekker, J. & Mirny, L. The 3D genome as moderator of chromosomal communication. *Cell* **164**, 1110–1121 (2016).
54. Yu, M. & Ren, B. The three-dimensional organization of mammalian genomes. *Annu. Rev. Cell Dev. Biol.* **33**, 265–289 (2017).
55. Ghosh, R. P. & Meyer, B. J. Spatial organization of chromatin: emergence of chromatin structure during development. *Annu. Rev. Cell Dev. Biol.* **37**, 199–232 (2021).
56. Wang, W. et al. TCF-1 promotes chromatin interactions across topologically associating domains in T cell progenitors. *Nat. Immunol.* **23**, 1052–1062 (2022).
57. Henning, A. N., Roychoudhuri, R. & Restifo, N. P. Epigenetic control of CD8(+) T cell differentiation. *Nat. Rev. Immunol.* **18**, 340–356 (2018).
58. Ramirez, R. N., Chowdhary, K., Leon, J., Mathis, D. & Benoist, C. FoxP3 associates with enhancer-promoter loops to regulate T(reg)-specific gene expression. *Sci. Immunol.* **7**, eabj9836 (2022).
59. Du, J. et al. FOXP3 exon 2 controls T(reg) stability and autoimmunity. *Sci. Immunol.* **7**, eabo5407 (2022).
60. Langmead, B. & Salzberg, S. L. Fast gapped-read alignment with Bowtie 2. *Nat. Methods* **9**, 357–359 (2012).
61. Tarasov, A., Vilella, A. J., Cuppen, E., Nijman, I. J. & Prins, P. Sambamba: fast processing of NGS alignment formats. *Bioinformatics* **31**, 2032–2034 (2015).
62. Chen, Q., Dai, J. & Bian, Q. Integration of 3D genome topology and local chromatin features uncovers enhancers underlying craniofacial-specific cartilage defects. *Sci. Adv.* **8**, eabo3648 (2022).
63. Labun, K. et al. CHOPCHOP v3: expanding the CRISPR web toolbox beyond genome editing. *Nucleic Acids Res.* **47**, W171–W174 (2019).

Acknowledgements

The authors thank the Flow Cytometry Lab and Bioimaging Facility at the Shanghai Institute of Precision Medicine. This work was supported by the National Natural Science Foundation of China (32170544, 32370607, and 31970585 to Q.B.) and the Natural Science Foundation of Shanghai (23ZR1435700). Q.B. is also supported by the Innovative Research Team of High-Level Local Universities in Shanghai (SHSMU-ZLCX20211700).

Author contributions

Q.B. conceived and designed research; B.W. performed experiments and analyzed data; Q.B. supervised experiments and data analysis; Q.B. and B.W. wrote the manuscript.

Competing interests

The authors declare no competing interests.

Additional information

Supplementary information The online version contains supplementary material available at https://doi.org/10.1038/s42003-024-07021-8.

Correspondence and requests for materials should be addressed to Qian Bian.

Peer review information *Communications Biology* thanks Bingtao Hao, Charalampos Spilianakis, and the other, anonymous, reviewer for their contribution to the peer review of this work. Primary Handling Editors: Dr Guideng Li and Dr Ophelia Bu. A peer review file is available.